Journal of Chromatography A 1618 (2020) 460849

Contents lists available at ScienceDirect

Journal of Chromatography A

journal homepage: www.elsevier.com/locate/chroma

Aging-related lipidomic changes in mouse serum, kidney, and heart by nanoflow ultrahigh-performance liquid chromatography-tandem mass spectrometry

Jung Yong Eum[a], Jong Cheol Lee[a], Sun Shin Yi[b,c], Il Yong Kim[c,d], Je Kyung Seong[c,d,*], Myeong Hee Moon[a,**]

[a] Department of Chemistry, Yonsei University, Seoul 03722, Republic of Korea
[b] Department of Biomedical Laboratory Science, College of Biomedical Sciences, Soonchunhyang University, Asan, Republic of Korea
[c] Korea Mouse Phenotyping Center, Seoul National University, Seoul, Republic of Korea
[d] Laboratory of Developmental Biology and Genetics, College of Veterinary Medicine, BK21 Program for Veterinary Science, BIO-MAX institute, Seoul National University, Seoul, Republic of Korea

ARTICLE INFO

Article history:
Received 19 October 2019
Revised 6 December 2019
Accepted 2 January 2020
Available online 3 January 2020

Keywords:
Lipidomics
Aging
Mouse
Kidney
Heart
nUHPLC-ESI-MS/MS

ABSTRACT

Aging refers to the intracellular accumulation of reactive oxygen species that damages proteins, DNA, and lipids. As alterations in lipid metabolism may trigger metabolic disorders and the onset of metabolic diseases, changes in lipid profiles can be closely related to aging. In this study, a comprehensive lipidomic comparison between 4- and 25-month-old mice was performed to investigate age-induced changes in the lipid profiles of mouse serum, kidney, and heart using nanoflow ultrahigh-performance liquid chromatography-electrospray ionization-tandem mass spectrometry. Quantitative analysis of 279 of the 542 identified lipids revealed significant changes upon aging, mainly showing decreased levels in the three types of samples. Exceptionally, most triacylglycerols showed significant increases in heart tissue. The kidney was influenced more by aging than the serum and heart. The highly abundant lipids in each lipid class with significant decreases ($>$ 2-fold, $p < 0.01$) were lysophosphatidic acid 18:1, lysophosphatidylinositol 20:4, and ceramide d:18:1/24:0 in serum; lysophosphatidylglycerol 16:0 in heart tissue; and eight phosphatidylethanolamines (20:4, 22:6, 36:2, 36:3, 38:4, 38:5, 38:6, 40:6, and 40:7), two cardiolipins (72:7 and 72:8), and lysophosphatidylcholine 18:0 in kidney tissue. The findings indicate the potential of lipidomic analysis to study characteristic age-related lipid changes.

© 2020 Elsevier B.V. All rights reserved.

1. Introduction

Aging is characterised in part by the progressive decline in metabolic function with increased risks of disease and death [1–4]. The global fertility rate and human life expectancy continue to decline and increase, respectively. However, the health life expectancy or 'healthspan' has not increased substantially. Elderly people who are sick can remain sick longer and simultaneously suffer from several chronic diseases [5]. As the global number of people over age 65 is expected to reach 1.6 billion by 2050, representing approximately 16.7% of the total global population of 9.4 billion [6], it is necessary to improve the healthspan through early diagnosis and prevention of diseases, as well as extension of life expectancy.

Aging in cells is generally characterised by decreased autophagic activity and the intracellular accumulation of reactive oxygen species (ROS) due to oxidative stress [7,8]. Oxidative damage to proteins, DNA, lipids, and subcellular species in cells play important roles in aging [9,10] and may cause age-related diseases such as diabetes, cardiovascular diseases, and neurodegenerative diseases among others [1,4,8]. Numerous efforts have sought to identify molecular biomarkers of aging including leukocyte telomere length, 8-hydroxydeoxyguanosine involved in DNA repair, growth hormone, and insulin-like growth factor [11–15]. In particular, alterations in lipid metabolism are reported to trigger metabolic disorders, such as diabetes and cardiovascular disease [16,17]. Lipid profiles including oxidised lipids are expected to be associated with aging. Several studies have explored the relationship between lipids and age-related diseases [18–21]. However, only a few studies have compared lipid changes with aging effects.

* Corresponding author at: Korea Mouse Phenotyping Center, Seoul National University, Seoul, Republic of Korea.
** Corresponding author.
E-mail addresses: snumouse@snu.ac.kr (J.K. Seong), mhmoon@yonsei.ac.kr (M.H. Moon).

https://doi.org/10.1016/j.chroma.2020.460849
0021-9673/© 2020 Elsevier B.V. All rights reserved.

These include assessments of continuous increase in triacylglycerol (TG) levels with age [22,23], cardiovascular disease and diabetes [24,25], and an increase in sphingomyelin (SM) levels in the amygdala and central nervous system of aged rats [26,27]. Since lipids play important roles in cell signalling in addition to energy storage and the maintenance of cellular structures, a comprehensive comparative lipidomic analysis at the molecular level is important to unveil the role of lipids in aging in the context of an improved healthspan.

Analysis of lipids is often complicated due to the diversity of their molecular structures. Based on structure, lipids are classified as glycerophospholipids, glycerolipids, sphingolipids, sterols, fatty acids, prenols, saccharolipids, and polyketides according to the LIPID MAPS nomenclature [28]. As lipid molecular structures vary with the polar head groups, length and degree of unsaturation of the acyl chain, and glycan attachment, lipidomic analysis in biological systems requires systematic determination of lipid molecular structures followed by targeted quantification. Liquid chromatography coupled with electrospray ionization-tandem mass spectrometry (LC-ESI-MS/MS) has been utilized as a powerful method to analyse complicated lipid mixtures in their intact condition [29–32]. The detection limit can often be lowered to a few femtomoles when incorporating capillary LC in a nanoflow rate regime [31]. Recently, the use of nanoflow ultrahigh performance LC with tandem MS (nUHPLC-ESI-MS/MS) facilitated lipid analysis with high-speed quantification (< 20 min) of several hundred lipids with the use of a selected reaction monitoring (SRM) method [33]. In our laboratory, this approach has been widely applied to study lipidomic alterations in the plasma of patients with Alzheimer's disease [21], in exosomes recovered from the urine of patients with prostate cancer [34], and from different brain regions of mice consuming a high fat diet [35].

In this study, the effect of aging on the lipid profiles of mice was investigated at the molecular level using nUHPLC-ESI-MS/MS. A comprehensive lipid analysis using the serum, heart tissue, and kidney tissue of 4- and 25-month-old C57BL/6 N mice was accomplished by non-targeted identification of lipid structures using data-dependent collision-induced dissociation experiments followed by SRM quantification of targeted lipid species. Age-associated changes in the lipidome of the two organs displaying the highest resting metabolic rates were examined for an increased understanding of the roles of lipids in the aging process and to assess lipidomic signatures for early detection or prediction of aging.

2. Experimental

2.1. Reagents

For the optimization of nUHPLC-ESI-MS/MS run conditions, a total of 33 lipid standards were utilized: LPC 12:0, LPC 16:0, PC 12:0/12:0, PC 16:0/16:0, PC P-18:0/22:6 (PC plasmalogen), LPE 14:0, LPE 18:0, PE 12:0/12:0, PE P-18:0/22:6, PE P-18:0/18:1, LPA 12:0, PA 18:0/18:0, LPG 18:0, PG 16:0/16:0, PG 18:0/18:0, LPI 18:0, LPI 20:4, PI 18:0/18:0, PI 18:0/20:4, LPS 16:0, LPS 18:1, PS 12:0/12:0, PS 16:0/18:1, PS 18:0/18:0, DG 16:0/18:1, TG 18:0/18:0/18:1, SM d18:1/16:0, HexCer d18:1/12:0, HexCer d18:1/16:0, SulfoHexCer d18:1/12:0, and CL 14:0/14:0/14:0/14:0 from Avanti Polar Lipids Inc. (Alabaster, AL, USA), and Cer d18:1/14:0 and Cer d18:1/22:0 from Matreya, LLC. (Pleasant Gap, PA, USA). CL 14:0/14:0/14:0/14:0 and the following 18 lipid standards with odd-numbered fatty acyl chains as non-endogenous lipids were used as internal standards added to lipid extract samples for targeted quantification: LPC 17:0, PC 13:0/13:0, LPE 17:1, PE 17:0/17:0, LPA 17:0, PA 17:0/17:0, LPG 17:1, PG 15:0/15:0, LPI 17:1, PI 12:0/13:0, LPS 17:1, PS 17:0/17:0, D_5-DG 17:0/17:0, D_5-TG 17:0/17:1/17:0, SM d18:1/17:0, Cer d18:1/17:0, HexCer d18:1/17:0, and SulfoHexCer d18:1/17:0 from Avanti Polar Lipids Inc. HPLC grade solvents including H_2O, acetonitrile (CH_3CN), methyl alcohol (CH_3OH), isopropanol, and methyl–*tert*–butyl ether (MTBE) were purchased from Avantor Performance Materials (Center Valley, PA, USA). Ammonium hydroxide (NH_4OH) and ammonium formate (NH_4HCO_2) used for ionization modifiers were purchased from Sigma-Aldrich (St. Louis, MO, USA). Fused silica capillary tubes with inner diameters of 20, 50, and 100 μm (outer diameter of 360 μm for all) were purchased from Polymicro Technology, LLC. (Phoenix, AZ, USA). The packing material used to prepare of a pulled-tip capillary column comprised 1.7 μm ethylene bridged hybrid (BEH) particles unpacked from an ACQUITY UPLC® BEH C18 column (2.1 mm × 100 mm) purchased from Waters™ (Milford, MA, USA).

2.2. Animals

C57BL/6 N female mice purchased from Central Lab. Animal Inc. (Seoul, Korea) were maintained in the animal facility at Korea Mouse Phenotyping Center, Seoul National University, for 4 months (young group, $n = 10$) and 25 months (aging group, $n = 9$). Animals of each group were sacrificed on the same day by inducing euthanasia using CO_2 gas and were perfused for quality control of tissue samples. After removing blood from the body through perfusion, the kidney and heart tissues were extracted. The left and right side of the kidney were collected separately, and both sides were mixed evenly for each sample. Animal experiments were conducted following the 'Guide for Animal Experiments', edited by the Korean Academy of Medical Sciences, and were approved by the Institutional Animal Care and Use Committee of Seoul National University. Body weight and weights of the kidney and heart were measured and are listed in Table S1.

2.3. Lipid extraction

Tissue samples were lyophilised before lipid extraction and then crushed into a fine powder. For non-targeted lipid identification, an equal portion of individual samples in each group were mixed to prepare a pooled sample as a representative of each group, including a total of 100 μL for serum and a total of 8 mg for the kidney and heart. For targeted lipid quantitation, individual animal samples (100 μL for serum and 8 mg for tissue from each animal) were used for lipid extraction. Individual serum samples were first dried in a model Bondiro MCFD 8508 freeze dryer vacuum centrifuge (IlShinBioBase, Yangju, Korea) and the lyophilized powder was mixed with 300 μL of methanol in an ice bath and incubated for 10 min. Individual tissue samples were each added to 150 μL of a 9:1 (v/v) solution of H_2O and phosphate-buffered saline and tip-sonicated for 1 min in an ice bath. Each mixture was dissolved in 300 μL CH_3OH in an ice bath and vortexed for 10 min. Following incubation for serum samples or vortexing for tissue samples, 1 mL of MTBE with 100 μL of MS-grade H_2O was added to each sample and the mixture was vortexed for 1 h [36]. After vortexing, the mixture was centrifuged at 1000 × g for 10 min and the organic layer was transferred to a new tube. The aqueous layer was mixed with 400 μL of MTBE and vortexed for 10 min at 1000 × g. The resulting organic layer was added to the previously collected extract. The organic solvent of the final mixture was removed using the freeze dryer vacuum centrifuge for 3 h. During evaporation, the tube was wrapped with a MillWrap PTFE membrane (0.45 μm; Millipore, Bedford, MA, USA) to minimise the loss of lipids. Dried lipid powders were re-constituted in $CHCl_3$:CH_3OH (1:9, v/v) at a concentration of 10 μg/μL and stored at −80 °C. For nUHPLC-ESI-MS/MS analysis, each stored lipid sample was further diluted to 2 μg/μL with CH_3OH:H_2O (9:1, v/v).

2.4. nUHPLC-ESI-MS/MS

Lipid analysis was performed using two sets of nUHPLC-ESI-MS/MS systems: a Dionex Ultimate 3000 RSLCnano System with LTQ Velos ion trap mass spectrometer from Thermo Fisher Scientific (San Jose, CA, USA) for non-targeted lipid identification and a nanoACQUITY UPLC system from Waters™ (Milford, MA, USA) coupled with a TSQ Vantage triple-stage quadrupole MS system from Thermo Fisher Scientific for targeted quantification. Analytical columns were prepared in the laboratory using fused silica capillary tubes (100 μm inner diameter (I.D.), 360 μm outer diameter, 7 cm long). Prior to packing, a capillary tube exposed to flame was extended and tapered to produce a sharp needle-like tip for the self-emitter in the MS experiment. The end portion (~ 5 mm) of the pulled-tip column was filled with 3 μm of 100 Å Watchers® ODS-P C-18 particles from (Isu Industry Corp., Seoul, Korea) to form a self-assembled frit and the rest (6.5-cm) was packed with 1.7-μm XBridge® BEH resin under nitrogen gas at 1000 psi. The capillary column was connected with a capillary tube (50 µm I.D.) from the nUHPLC pump via a PEEK micro-cross (IDEX Health & Science, Oak Harbor, WA, USA). The other two ports of the micro-cross were connected with a pressure capillary tube (20 µm I.D.) and an on/off switching valve to split the pump flow. For binary gradient elution, the same set of mobile phase solutions was used for both nUHPLC systems: H_2O:CH_3CN (9:1, v/v) for mobile phase A and CH_3OH:CH_3CN:IPA (2:2:6, v/v) for mobile phase B. Both solutions were added with a mixture of ionization modifiers, 0.05% NH_4OH and 5 mM NH_4HCO_2, which are universal for both positive and negative ion modes of MS detection.

Non-targeted lipid identification was carried out with pooled lipid extracts. For each sample group, 3 μg of lipid extract was loaded onto the analytical column from an autosampler using mobile phase A at a flow rate of 1.0 μL/min for 7 min. Gradient elution began with 60% of mobile phase B at a pump flow rate adjusted to 9 μL/min with the switching valve on for flow splitting to deliver 300 nL/min to the analytical column. Mobile phase B was ramped up to 80% for 11 min, raised to 100% for 20 min, and maintained for 7 min at 100%. Then, mobile phase B was decreased to 0% (100% A) and re-equilibrated for 10 min prior to the next run. The m/z range of a precursor MS scan was set to 300–1000 m/z for lipid detection in which range CL species were detected as $[M\text{-}2H]^{2-}$ form. The ESI voltage was set to 3.0 kV for both positive and negative ion modes. For data-dependent MS/MS experiments, 40% normalized collision energy was utilized. The lipid molecular structures were identified with LiPilot, a PC-based software created in our laboratory [37]. Targeted quantification of lipids was performed with each lipid extract of an individual animal, which was added along with 19 internal standards (ISs). For each injection, 2 μg of lipid extracts containing 1 pmol of each IS were loaded onto the same analytical column with mobile phase A for 7 min at 1 μL/min. After sample loading, the switching valve was adjusted to the split mode and the total pump flow rate was set at 16 μL/min (300 nL/min for analytical column). Gradient elution began at 60% B, was ramped to 100% for 20 min, maintained at 100% B for 4 min, and resumed at 100% A. For quantification of lipids, SRM-based analysis was performed by scanning the precursor ion and a selected product ion in data-dependent CID experiments in the polarity switching mode (alternating detection at positive and negative ion mode) of the triple-stage quadrupole MS system. This involved LPC, PC, LPE, PE, DG, TG, SM, Cer, HexCer, and SulfoHexCer in the positive ion mode and LPA, LPG, PG, LPI, PI, LPS, PS, MLCL, and CL in the negative ion mode. For SRM quantification, each lipid class was assigned different CID energies: 20 V for LPE, PE (except PEp), and LPS; 30 V for LPA, PA, LPG, PG, LPI, DG, TG, Cer, HexCer, and SulfoHexCer; 35 V for PS; 40 V for LPC, PC, PEp, SM, and CL as listed in Table S2 along with the type of precursor and quantifier ion of each lipid class. The amounts of individual lipid species were determined by calculating the corrected peak area (the ratio of the peak area of a species to the area of the IS specific to each lipid class), which is a good estimate of the pmol/mg for tissue sample. Serum lipid levels were normalized to the sample volume following the recently established guidelines for MS-based lipidomics for blood [38]. Student's *t*-test was performed with SPSS software (version 20.0, IBM Corp., Armonk, NY, USA) and the principal component analysis (PCA) was performed using Minitab 17 statistical software (http://www.minitab.com).

3. Results

3.1. Non-targeted identification and SRM quantification

Structural determination of lipids from mouse samples was conducted using nUHPLC-ESI-MS/MS in run conditions optimized with a mixture of lipid standards as shown in Fig. 1. Base peak chromatograms (BPCs) demonstrated the high-performance lipid separation by the homemade column: 14.0 ± 4.2 s for the average peak width and 0.5 ± 0.3% for the average RSD in retention time of all standards. Determinations of lipid molecular structures were made from fragment ion spectra obtained by a data-dependent CID experiment. An example is the PC plasmalogen (PC P-18:0/22:6, peak # 10 in Fig. 1a) in Fig. 2, which shows (a) the chromatogram and (b) data-dependent CID spectra of the parent ion (*m/z* 818.6) obtained at 19.49 min. Fragment ion spectra shows the dissociation of the acyl chain in the form of ketene at *m/z* 491.5 (**1**, $[M + H\text{-RCH=}C = O]^+$) and the dissociation of an ether-linked alkyl chain at *m/z* 550.5 (**2**, $[M + H\text{-R}^{'}\text{CH=CHOH}]^+$)

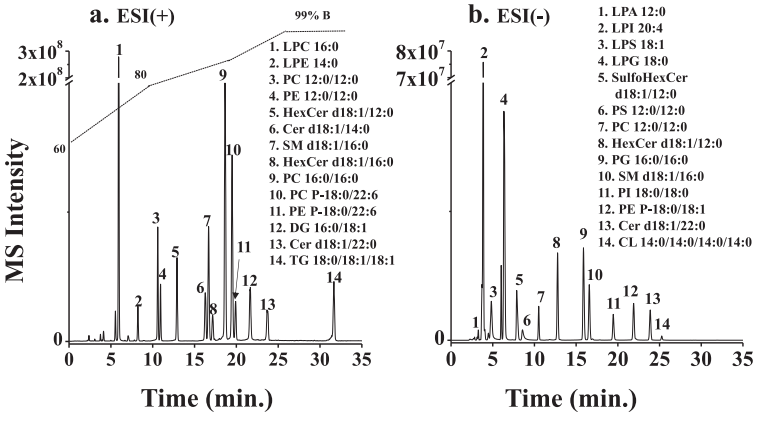

Fig. 1. Base peak chromatograms (BPCs) of lipid standards in (a) positive and (b) negative modes of nUHPLC-ESI-MS/MS. Both runs used the same gradient condition (%, B).

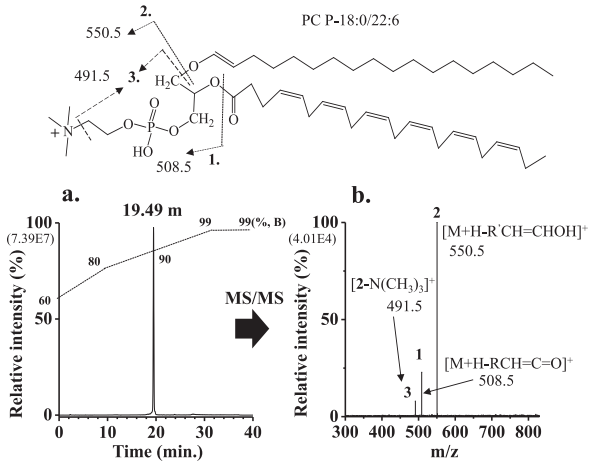

Fig. 2. Structural determination of PC P-18:0/22:6 standard in the positive ion mode of nUHPLC-ESI-MS/MS: (a) an extracted ion chromatogram (EIC) and (b) MS/MS spectra with the fragment ion pattern in the molecular structure (top).

along with further loss of trimethylamine at *m/z* 508.5 (3, [*M* + *H*-R'CH=CHOH–$N(CH_3)_3^+$]). Non-targeted lipid identification of the lipid extract samples (serum, kidney tissue, and heart tissue from young and old mice) was performed under the same run conditions used in Fig. 1 and their BPCs are shown in Fig. S1.

A total of 542 unique lipids from all sample groups were identified with their molecular structures. Of these, only 279 lipids were quantified by SRM using nUHPLC with triple quadrupole MS. The limit of detection (LOD, 3 × *s*/m) and the limit of quantitation (LOQ, 10 × s/m) values of lipid standard of each lipid class were calculated from the calibration curves of standards spiked to each type of samples (s for standard deviation of the y intercept and m for the slope of the calibration curve) and are listed in Table S3. Briefly, LOD/LOQ values ranged from 0.011/ 0.038 pmol for PG 15:0/15:0 to 0.071/0.236 pmol for CL 14:0/14:0/14:0/14:0 when spiked to serum and the calibration curves are in Fig. S2. The matrix effects were assessed by spiking internal standards to sample lipid extracts as 82.2 ~ 119.2% and the relative standard deviation (RSD,%) was lower than 14.8 as listed in Table S4. The intra-day and inter-day variations were measured by analyzing the internal standard mixture between the sequence of targeted quantitation by nUHPLC-ESI-MS/MS. RSD values of the intra-day and the inter-day variations were less than 12.9 and 11.5%, respectively, and the relative error (RE,%) values were less than 14.0 and 12.6% as listed in Table S5.

Table S6 lists the lipid amount of each quantified lipid species from individual animals compared between the young and aging groups for the three sample types. The data for% (Y) in Table S6 represents the relative abundance of each species in the corresponding lipid class based on the young group data. Values marked in bold are high-abundance species in which high-abundance was defined as a lipid with a relative abundance higher than 100% divided by the lipid numbers in the class. Among lipid classes, PC, PE, TG, and CL were quantified by the total number of carbons and double bonds. The information concerning the identified isomeric chain structures is listed in Table S7.

3.2. Perturbations in lipid profiles upon aging

Overall changes in the individual lipid levels of mice upon aging were viewed using Volcano plots of -$\log_{10}$ (*p*-value) *vs.* $\log_2$ (fold-change (A/Y)). In Fig. 3, the data points in the upper left and upper right regions are lipids that displayed significant > 2-fold decreases and increases ($p < 0.01$), respectively. Few lipid species in serum were decreased. However, in the kidney tissue, many lipids were significantly decreased, and some were significantly increased. However, more lipids were increased in the heart tissue of older mice. Detailed changes in lipid class and individual lipid species are illustrated in the stacked bar graph in Fig. S3. Eight of 15 lipid classes (LPC, PE, PI, PS, TG, SM, Cer, and CL) examined in this study exhibited > 2-fold changes among one of the three sample types in the aging group. Chain structures marked in the right of each bar of Fig. S3 were high-abundance species in each lipid class with the remaining species designated as “low”. Variation in the total amount of lipid classes was visualised in Fig. 4 by plotting the fold changes (A/Y) in each lipid class obtained by calculating the ratio of the summed amounts of lipids in each class between young and aging mice. Apparently, LPI, SM, Cer, and HexCer in the serum, and LPC, LPE, PE, PS, and CL in the kidney were significantly reduced (> 2-fold, $p < 0.01$) in the aging group compared to the young group. A large increase in TG ($p < 0.05$) was observed in the heart tissue of the aging group. The reason for the relatively high *p*-value for TG species will be explained later.

Among the 279 quantified species, lipids showing significant changes (> 2-fold, $p < 0.01$) including low abundance species were plotted on a heat map (Fig. 5). All the serum lipids in Fig. 5a were lowered upon aging and most kidney lipids in Fig. 5b were significantly lowered, except for several TG and a Cer. Although most lipid species showing significant changes exhibited decreased levels, seven TG species in heart tissue were increased in the aging group. The overall change was further illustrated with the PCA plot in Fig. 6. Data points representing the lipid profiles of the heart and kidney of individual animals were clustered away from those in the young group, whereas alterations in the serum lipid profiles were not significant. These observations support the view that alterations in the lipid profiles of the heart and kidney tissues of the aging group were relatively larger than those of serum.

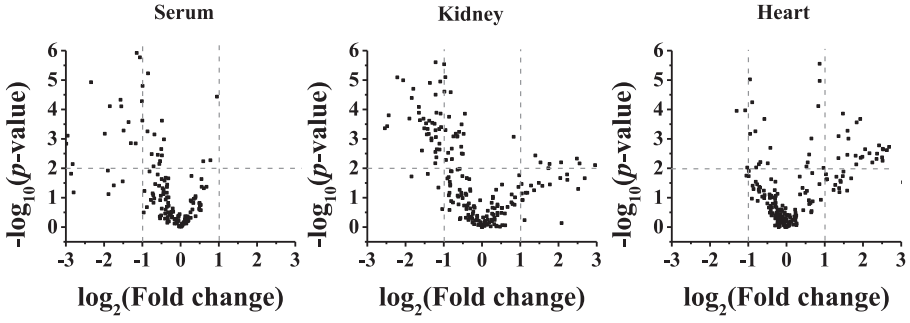

Fig. 3. Volcano plots of quantified lipid species (163 from serum, 204 from kidney, and 201 from heart) showing differences in the serum, kidney tissue, and heart tissue between the aging and young groups. The horizontal border line in each Volcano plot represents $p = 0.01$, and the two vertical lines represent a 2-fold increase (+1) and decrease (−1) in the fold-change (aging/young), respectively.

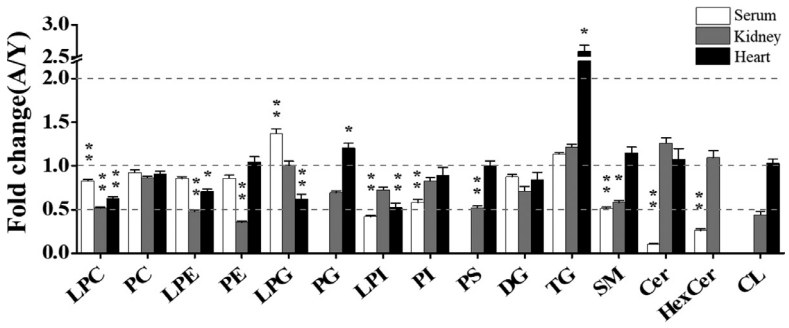

Fig. 4. The fold-change (A/Y) in the total amount of lipids in each lipid class ($^{*}p < 0.05$, $^{**}p < 0.01$).

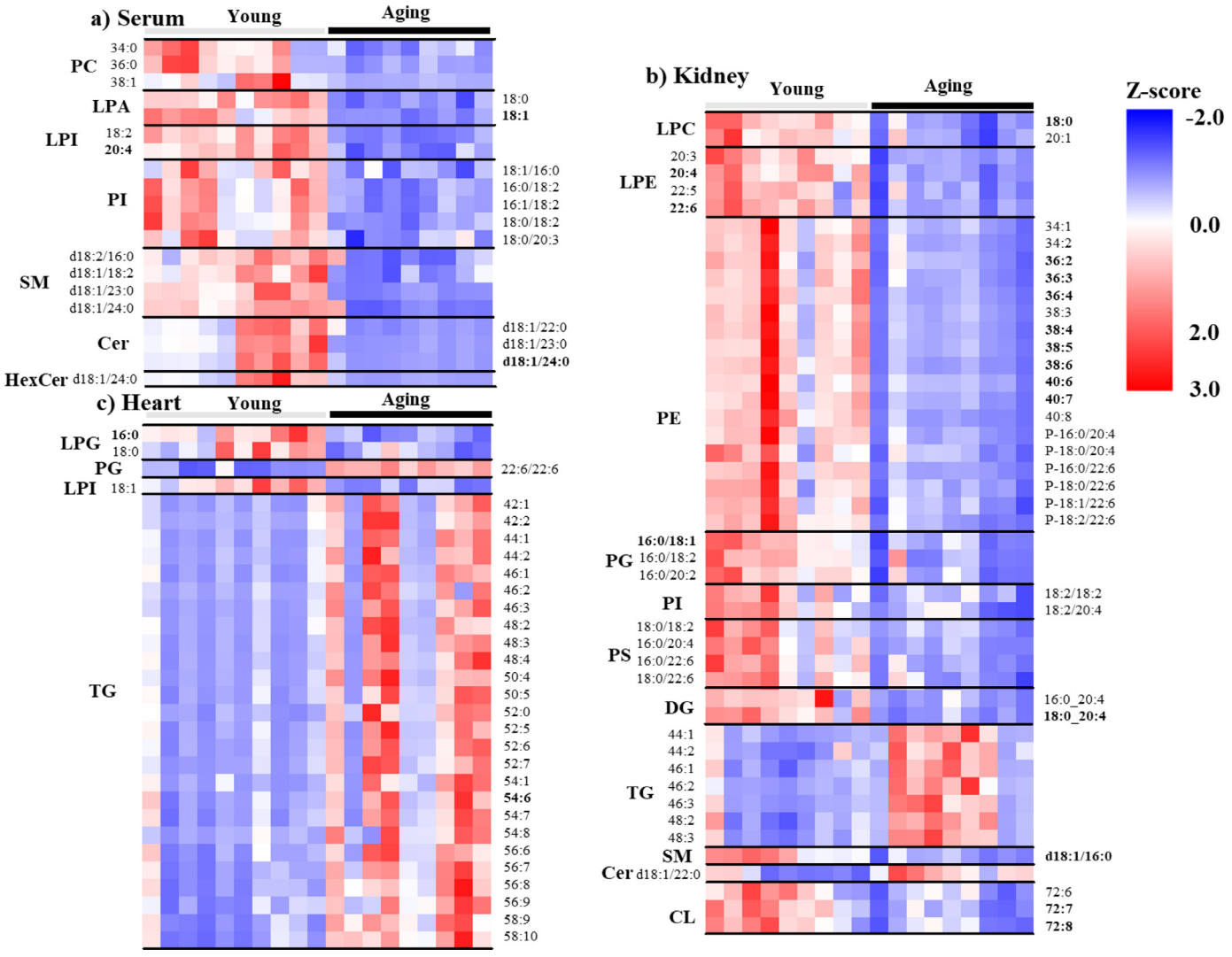

Fig. 5. Heat map of lipid species showing significant changes (> 2-fold, $p < 0.01$) in the aging group compared to the young group. Species marked with bold numbers of acyl chain structures are high-abundance species in each lipid class.

Variations at individual lipid levels were plotted by sorting out the high-abundance lipids in each class with significant differences (* for $p < 0.05$ and ** for $p < 0.01$) in Fig. S4. As observed in the PCA plot of serum samples, only PI 18:0/20:4 and three SM species (d18:1/16:0, d18:2/16:0, and d18:1/24:1) were significantly ($p < 0.01$) reduced. In case of the kidney, two LPC species (18:0 and 18:2), PE (38:4 and 40:6), CL (72:7 and 72:8), and SM d18:1/16:0 were significantly reduced. Though five TG species (50:2, 52:4, 54:2, 54:3, and 54:4) were markedly increased (> 2-fold) in the heart tissue, their p values were not statistically significant (< 0.05) because three mice in the aging group did not show increases in TG levels (Fig. 5c), whereas the other six animals showed remarkable increases.

The ratio of the total amounts of PC to PE (PC/PE) was examined in the kidney and heart tissues upon aging (Fig. 7a). The average PC/PE in the kidney was significantly ($p < 0.01$) increased in the aging group, whereas the difference in the heart was not statistically significant. This is supported by the fold ratio (A/Y) of nine

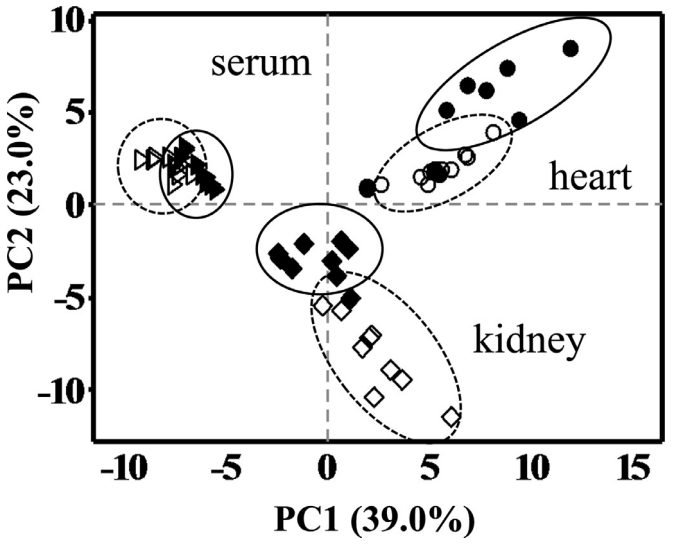

Fig. 6. Principal component analysis (PCA) plots showing differences in lipid profiles between the aging and young groups. Plots are based on lipid species showing significant differences (> 2-fold and p-value < 0.01).

PE species in Fig. 7b, which were largely reduced only in the kidney, whereas changes in the total amount of PC upon aging were negligible (Fig S5).

Changes in plasmalogen lipids, which protect cells against damage from ROS, were investigated by plotting the fold-change (A/Y) of five PC plasmalogen (PCp) and five PE plasmalogen (PEp) species. As shown in Fig. S6, although the overall amounts of plasmalogen in the serum, kidney tissue, and heart tissue did not appear to be altered, significant decreases (> 2-fold, $p < 0.01$) were found in four PEp species in kidney tissue upon aging, whereas PC P-18:1 was increased to some degree in kidney tissue. More substantial alterations in plasmalogen lipid levels upon aging were found in PEp than PCp and in kidney tissue than in heart tissue.

Quantified results were further screened to select high-abundance lipid species showing significant differences (> 2-fold and $p < 0.01$). They included 3, 16, and 2 in the serum, kidney tissue, and heart tissue of the aging group, respectively (Table 1). The lipids presented in this table showed statistical differences of $p < 0.001$, except for the three species marked with ** indicating $p < 0.01$. In serum, LPA 18:1 and LPI 20:4 were reduced by half, but Cer d:18:1/24:0 was significantly reduced by >10-fold in the aging group. In case of kidney tissue, a considerable number of lipids [LPC 18:0, nine PE species including two LPE, PG 16:0/18:1, DG 18:0_20:4, SM d18:1/16:0, and two CL (72:7 and 72:8)] were reduced. The underdash '_' in the acyl chain information of DG was used between the two acyl chain structures because the exact chain locations could not be completely resolved, whereas '/' was used for lipids when the acyl chain locations at sn-1 and sn-2 could be differentiated by MS/MS spectra. However, TG 54:6 was significantly accumulated (3.5-fold) in the heart tissue of the aging group, whereas LPG 16:0 was reduced by more than 2-fold.

4. Discussion

Lipid alterations found in the serum, kidney, and heart tissues of aged mice in this study can be compared with those in literature describing lipidomic perturbations in age-related disease. Overall LPC levels were significantly ($p < 0.01$) decreased in the kidney and heart tissues of aged mice. Although the decrease in serum was only approximately 20%, it was statistically significant ($p < 0.01$) and similar to the decrease of LPC levels in the plasma of patients with metabolic syndrome [39].

PE is the second most abundant glycerophospholipid after PC in mitochondria and is important for mitochondrial function during the aging process [40]. Reduction in the levels of PE compromises the membrane fluidity of mitochondria, which results in reduced respiratory capacity and impaired fusion and fission, leading to accelerated aging [41–43]. Deficiency of PE by only 20–30% in mammalian mitochondria impairs cell growth and ATP synthesis [40]. The levels of most PE species from the skeletal muscle mitochondria of old (78-week-old) mice can be significantly reduced [42]. In this study, 18 of 26 identified PE species showed significantly reduced levels in the aged kidney, whereas negligible changes were observed for these in the heart tissue and serum. There are two pathways involved in the synthesis of the majority of PE in mammalian cells: the CDP-ethanolamine pathway on the endoplasmic reticulum (ER) and the phosphatidylserine decarboxylase (PSD) pathway in the mitochondrial inner membrane [42]. Since most PE in mammalian mitochondria are produced from PS by PSD, reduced PS levels could result in decreased PE [40]. However, a study on the relationship between aging and PE levels postulated that reduction of PE levels by depletion of PSD activity accelerated the production of age-related ROS and death [44]. Because the relationship between decreased PE levels and aging has been revealed by few studies only, the decrease in PS cannot be clearly correlated with PE at present. However, the present study also showed significant reduction (~ 2 fold) in PS levels in kidney along with a decrease in most PE species.

Similarly, levels of high-abundance CL species (72:6, 72:7, and 72:8) were reduced in the kidney, but there were no changes in most CLs in the heart tissue. Kidney tissue has the second highest mitochondrial content after heart tissue and requires sufficient energy from mitochondria for waste removal from the blood, reabsorption of nutrients, balancing electrolytes, and maintaining

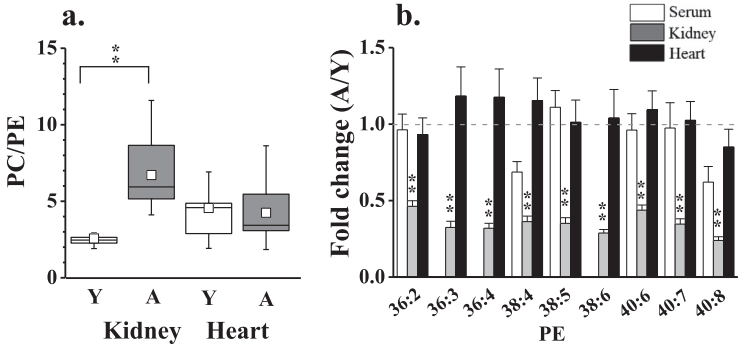

Fig. 7. a) PC/PE ratios between the aging (A) and young (Y) groups based on the corrected peak area (*vs.* IS) in the kidney and heart and b) the fold changes (A/Y) of individual PE species from the serum, kidney, and heart. (**$p < 0.01$).

Table 1
High-abundance lipid species altered significantly (>2-fold and $p < 0.001$, except for § with $p < 0.01$) in the serum, kidney tissue, and heart tissue of the aging group, represented with fold-change (A/Y) and the relative abundance in each lipid class.

	Class	Chain structure	*m/z*	Abundance% (Y)	Fold-change (A/Y)	*p*-value
Serum	LPA	18:1	435.5	70.1	0.48 ± 0.04	0.000002
	LPI	20:4	619.5	71.9	0.45 ± 0.02	0.000001
	Cer	d18:1/24:0	650.5	45.9	0.08 ± 0.01	0.000487
Kidney	LPC	18:0	524.5	25.2	0.39 ± 0.03	0.000013
	LPE	20:4	502.5	29.7	0.43 ± 0.03	0.000002
		22:6	526.5	25.8	0.43 ± 0.02	0.000031
	PE	36:2	744.5	4.6	0.46 ± 0.04	0.001453 §
		36:3	742.5	5.0	0.32 ± 0.04	0.000231
		36:4	740.5	10.0	0.32 ± 0.03	0.000130
		38:4	768.5	30.9	0.36 ±0.04	0.000296
		38:5	766.5	15.7	0.35 ± 0.04	0.000437
		38:6	764.5	8.9	0.29 ± 0.02	0.000020
		40:6	792.5	6.8	0.44 ± 0.03	0.004231
		40:7	790.5	6.5	0.35 ± 0.03	0.000206
	PG	16:0/18:1	747.5	23.3	0.47 ± 0.03	0.000138
	DG	18:0_20:4	662.5	17.3	0.22 ± 0.03	0.000008
	SM	d18:1/16:0	703.5	57.7	0.44 ± 0.03	0.000129
	CL	72:7	724.5	37.9	0.38 ± 0.06	0.000242
		72:8	737.5	43.1	0.46 ± 0.07	0.002300 §
Heart	LPG	16:0	483.5	51.1	0.41 ± 0.06	0.000112
	TG	54:6	896.5	2.9	3.54 ± 0.34	0.007357 §

acid-base homeostasis [45–47]. CL is the characteristic glycerophospholipid exclusively located in the inner mitochondrial membrane and is involved in maintaining membrane fluidity, generating ATP, and controlling the activity of cytochrome C oxidase during apoptosis [48,49]. Because increased levels of oxidative stress and CL deficiency have been implicated in the mitochondrial dysfunction associated with several pathophysiological conditions, including diabetes, heart failure, neurodegeneration, and aging [48–50], decrease in the level of high-abundance CLs in the kidney may imply that kidney is more influenced by aging than the heart.

Plasmalogens protect unsaturated lipid chain structures against oxidative damage by ROS [51]. In this study, four PEp species were significantly reduced in the kidney, but no change in heart tissue was noted. Reductions of PE, CL, and PEp were found in the kidney, whereas changes of these species in heart tissue were negligible, supporting the view that the lipid levels of the kidney were more affected by aging than those in the heart. PC/PE ratio was reported as an indicator of cell membrane integrity and the progression of steatohepatitis, in which liver failure was associated with a decreased PC/PE ratio due to the depletion of hepatic PC [52]. A recent study on the skeletal muscle lipids upon a high fat diet showed increased levels of PE leading to a decrease in the PC/PE and suggested that an abnormally high or low PC/PE ratio can be harmful, and that the PC/PE balance should be maintained [53]. However, aged mice of our study showed an opposite trend in which the PC/PE ratio was increased in kidney due to a significant reduction in PE levels, whereas PC levels were not altered. While the PC/PE ratio did not change in the heart due to negligible changes in both the PC and PE levels of heart tissue, the significant increase in the PC/PE ratio in the kidney can be a characteristic factor of kidney the caused by the age-related depletion of PE, that may impair respiratory capacity and eventually disturb cell integrity.

PI has an anti-inflammatory role as PI delivers arachidonic acid (20:4), a precursor of eicosanoids, which are inflammatory mediators, by regulating immune responses [54,55]. In this work, more than 70% of all PIs in the serum, kidney tissue, and heart tissue contained arachidonic acid. In aged mice, the total PI level was decreased in the serum, but not in the kidney and heart tissues. Moreover, the most abundant PI 18:0/20:4 was significantly reduced in serum. These results suggest that the decline of anti-inflammatory roles upon aging can be related with the reduced levels of serum PI containing an arachidonic acyl chain.

TG is strongly related with metabolic diseases including type 2 diabetes, cardiovascular disease, non-alcoholic fatty liver disease, and obesity with TG accumulation in blood and tissues [22,25,56]. In particular, TGs were reported to be accumulated in tissues rich with mitochondria in aged rats, such as the muscle, heart, and liver, but not in the kidney because TG accumulation was caused by the impaired mitochondrial function, which was induced by decreased mitochondrial fusion and autophagic disruption [56]. We observed a similar trend with significant accumulation of most TG species in heart tissue, but not in kidney tissue, supporting that TG accumulation in the heart is a characteristic change in heart tissue lipids upon aging. It is also noted that PG 22:6/22:6, presumably a bis(monoacylglycero)phosphate, which is a structural isomer of PG with each acyl chain attached to its two glycerol units, was increased in the heart tissue of aged mice.

In conclusion, we conducted a systematic examination of lipid alterations at the levels of both lipid classes and individual lipid molecules in the serum, kidney, and heart tissues between 4- and 25-month-old mice. Lipidomic analysis of serum and the two tissues revealed decreasing patterns for most lipid classes except for TG, which was increased in heart tissue upon aging. Among the lipid species showing significant decreases, critical changes were found for LPA 18:1, LPI 20:4, and Cer d:18:1/24:0 in the serum and LPG 16:0 in heart. Decreases in kidney lipids were found among broad lipid classes, LPC 18:0, LPE (20:4 and 22:6), CL (72:7 and 72:8), and six high-abundance PE species (36:2, 36:3, 38:4, 38:5, 38:6, 40:6, and 40:7), which were reduced by 2~3-fold and resulted in a decreased PC/PE ratio; however, the PC/PE ratio in the heart was not altered. Moreover, significant decreases were observed at the level of lipid class, such as LPC, LPE, PE, PS, and CL (> 2-fold) in kidney. Though the kidney and heart tissues displayed the highest resting metabolic rates [57], the present results suggest that lipid metabolism in the kidney is more influenced by aging than that in the heart.

Although the current study aimed to evaluate lipidomic alterations observed upon aging by selecting the two energy-demanding organs related to metabolic diseases, the results indicate the potential of lipidomic profiling to investigate age-related

changes in lipids, which can be utilized to develop possible lipid signatures in order to distinguish the physiological status of aging. Future studies on the development of lipidomic signatures for the early detection of aging and on lipid changes induced by aging will be performed in the presence and absence of physical exercise in an animal model.

Declaration of Competing Interest

The authors declare that they have no known competing financial interests or personal relationships that could have appeared to influence the work reported in this paper.

CRediT authorship contribution statement

Jung Yong Eum: Formal analysis, Data curation. **Jong Cheol Lee:** Data curation, Software. **Sun Shin Yi:** Resources. **Il Yong Kim:** Resources. **Je Kyung Seong:** Writing - review & editing. **Myeong Hee Moon:** Supervision, Writing - original draft.

Acknowledgements

This study was supported by Korea Mouse Phenotyping project (NRF-2017M3A9D5A01052447) and in part by a grant (NRF-2018R1A2A1A05019794) of the Ministry of Science, ICT & Future Planning through the National Research Foundation (NRF) of Korea. Mouse samples were provided by the Korea Mouse Phenotyping Center.

Supplementary materials

Supplementary material associated with this article can be found, in the online version, at doi:10.1016/j.chroma.2020.460849.

References

[1] N. Barzilai, D.M. Huffman, R.H. Muzumdar, A. Bartke, The critical role of metabolic pathways in aging, Diabetes 61 (2012) 1315–1322.
[2] T.B.L. Kirkwood, Understanding ageing from an evolutionary perspective, J. Intern. Med. 263 (2008) 117–127.
[3] T.B.L. Kirkwood, S.N. Austad, Why do we age? Nature 408 (2000) 233–238.
[4] J.E. Morley, Diabetes and aging: epidemiologic overview, Clin. Geriatr. Med. 24 (2008) 395 -+.
[5] B.K. Kennedy, S.L. Berger, A. Brunet, J. Campisi, A.M. Cuervo, E.S. Epel, C. Franceschi, G.J. Lithgow, R.I. Morimoto, J.E. Pessin, T.A. Rando, A. Richardson, E.E. Schadt, T. Wyss-Coray, F. Sierra, Geroscience: linking aging to chronic disease, Cell 159 (2014) 709–713.
[6] W. He, D. Goodkind, P. Kowal, in: An Aging world:2015, U.S. Census Bureau, 2016, pp. 3–37.
[7] A.M. Cuervo, E. Bergamini, U.T. Brunk, W. Droge, M. Ffrench, A. Terman, Autophagy and aging: the importance of maintaining "clean" cells, Autophagy 1 (2005) 131–140.
[8] K. Rahman, Studies on free radicals, antioxidants, and co-factors, Clin. Interv. Aging. 2 (2007) 219–236.
[9] G.M. Martin, S.N. Austad, T.E. Johnson, Genetic analysis of ageing: role of oxidative damage and environmental stresses, Nat Genet 13 (1996) 25–34.
[10] E.R. Stadtman, Protein oxidation in aging and age-related diseases, Ann. NY. Acad. Sci. 928 (2001) 22–38.
[11] P.M. Engelfriet, E.H.J.M. Jansen, H.S.J. Picavet, M.E.T. Doile, Biochemical markers of aging for longitudinal studies in humans, Epidemiol. Rev. 35 (2013) 132–151.
[12] H.D. Zhu, M. Belcher, P. van der Harst, Healthy aging and disease: role for telomere biology? Clin. Sci. 120 (2011) 427–440.
[13] S. Loft, K. Vistisen, M. Ewertz, A. Tjonneland, K. Overvad, H.E. Poulsen, Oxidative dna damage estimated by 8-Hydroxydeoxyguanosine excretion in humans - Influence of smoking, gender and body-mass index, Carcinogenesis 13 (1992) 2241–2247.
[14] H.S. Chahal, W.M. Drake, The endocrine system and ageing, J. Pathol. 211 (2007) 173–180.
[15] M. Sherlock, A.A. Toogood, Aging and the growth hormone/insulin like growth factor-I axis, Pituitary 10 (2007) 189–203.
[16] P.J. Meikle, G. Wong, C.K. Barlow, B.A. Kingwell, Lipidomics: potential role in risk prediction and therapeutic monitoring for diabetes and cardiovascular disease, Pharmacol. Ther. 143 (2014) 12–23.
[17] S. Pati, S. Krishna, J.H. Lee, M.K. Ross, C.B. de La Serre, D.A. Harn Jr., J.J. Wagner, N.M. Filipov, B.S. Cummings, Effects of high-fat diet and age on the blood lipidome and circulating endocannabinoids of female C57BL/6 mice, Biochim. Biophys. Acta Mol. Cell Biol. Lipids 1863 (2018) 26–39.
[18] R. Meshkani, K. Adeli, Hepatic insulin resistance, metabolic syndrome and cardiovascular disease, Clin. Biochem. 42 (2009) 1331–1346.
[19] L. Slama, C. Le Camus, L. Serfaty, G. Pialoux, J. Capeau, S. Gharakhanian, Metabolic disorders and chronic viral disease: the case of HIV and HCV, Diabetes Metab 35 (2009) 1–11.
[20] J.Y. Lee, S.K. Byeon, M.H. Moon, Profiling of oxidized phospholipids in lipoproteins from patients with coronary artery disease by hollow fiber flow field-flow fractionation and nanoflow liquid chromatography-tandem mass spectrometry, Anal. Chem. 87 (2015) 1266–1273.
[21] S.H. Kim, J.S. Yang, J.C. Lee, J.Y. Lee, J.Y. Lee, E. Kim, M.H. Moon, Lipidomic alterations in lipoproteins of patients with mild cognitive impairment and alzheimer's disease by asymmetrical flow field-flow fractionation and nanoflow ultrahigh performance liquid chromatography-tandem mass spectrometry, J. Chromatogr. A 1568 (2018) 91–100.
[22] L.A. Menahan, Age-related changes in lipid and carbohydrate metabolism of the genetically obese mouse, Metabolism 32 (1983) 172–178.
[23] D.A. Glei, N. Goldman, Y.H. Lin, M. Weinstein, Age-Related changes in biomarkers: longitudinal data from a population-based sample, Res Aging 33 (2011) 312–326.
[24] E.P. Rhee, S. Cheng, M.G. Larson, G.A. Walford, G.D. Lewis, E. McCabe, E. Yang, L. Farrell, C.S. Fox, C.J. O'Donnell, S.A. Carr, R.S. Vasan, J.C. Florez, C.B. Clish, T.J. Wang, R.E. Gerszten, Lipid profiling identifies a triacylglycerol signature of insulin resistance and improves diabetes prediction in humans, J. Clin. Invest. 121 (2011) 1402–1411.
[25] F. Sanders, B. McNally, J.L. Griffin, Blood triacylglycerols: a lipidomic window on diet and disease, Biochem. Soc. T 44 (2016) 638–644.
[26] R.G. Cutler, M.P. Mattson, Sphingomyelin and ceramide as regulators of development and lifespan, Mech. Ageing. Dev. 122 (2001) 895–908.
[27] R. Smidak, H.C. Kofeler, H. Hoeger, G. Lubec, Comprehensive identification of age-related lipidome changes in rat amygdala during normal aging, PLoS One 12 (2017) e0180675.
[28] E. Fahy, S. Subramaniam, H.A. Brown, C.K. Glass, A.H. Merrill Jr., R.C. Murphy, C.R. Raetz, D.W. Russell, Y. Seyama, W. Shaw, T. Shimizu, F. Spener, G. van Meer, M.S. VanNieuwenhze, S.H. White, J.L. Witztum, E.A. Dennis, A comprehensive classification system for lipids, J. Lipid. Res. 46 (2005) 839–861.
[29] R. Taguchi, J. Hayakawa, Y. Takeuchi, M. Ishida, Two-dimensional analysis of phospholipids by capillary liquid chromatography/electrospray ionization mass spectrometry, J. Mass. Spectrom. 35 (2000) 953–966.
[30] R. Taguchi, T. Houjou, H. Nakanishi, T. Yamazaki, M. Ishida, M. Imagawa, T. Shimizu, Focused lipidomics by tandem mass spectrometry, J. Chromatogr. B Analyt. Technol. Biomed. Life Sci. 823 (2005) 26–36.
[31] D.Y. Bang, M.H. Moon, On-line two-dimensional capillary strong anion exchange/reversed phase liquid chromatography-tandem mass spectrometry for comprehensive lipid analysis, J. Chromatogr. A 1310 (2013) 82–90.
[32] P.D. Rainville, C.L. Stumpf, J.P. Shockcor, R.S. Plumb, J.K. Nicholson, Novel application of reversed-phase uplc-oatof-ms for lipid analysis in complex biological mixtures: a new tool for lipidomics, J. Proteome Res. 6 (2007) 552–558.
[33] S.K. Byeon, J.C. Lee, B.C. Chung, H.S. Seo, M.H. Moon, High-throughput and rapid quantification of lipids by nanoflow UPLC-ESI-MS/MS: application to the hepatic lipids of rabbits with nonalcoholic fatty liver disease, Anal. Bioanal. Chem. 408 (2016) 4975–4985.
[34] J.S. Yang, J.C. Lee, S.K. Byeon, K.H. Rha, M.H. Moon, Size dependent lipidomic analysis of urinary exosomes from patients with prostate cancer by flow field--flow fractionation and nanoflow liquid chromatography-tandem mass spectrometry, Anal. Chem. 89 (2017) 2488–2496.
[35] J.C. Lee, S.M. Park, I.Y. Kim, H. Sung, J.K. Seong, M.H. Moon, High-fat diet-induced lipidome perturbations in the cortex, hippocampus, hypothalamus, and olfactory bulb of mice, Biochim. Biophys. Acta 1863 (2018) 980–990.
[36] S.K. Byeon, J.Y. Lee, M.H. Moon, Optimized extraction of phospholipids and lysophospholipids for nanoflow liquid chromatography-electrospray ionization-tandem mass spectrometry, Analyst 137 (2012) 451–458.
[37] S. Lim, S.K. Byeon, J.Y. Lee, M.H. Moon, Computational approach to structural identification of phospholipids using raw mass spectra from nanoflow liquid chromatography-electrospray ionization-tandem mass spectrometry, J. Mass Spectrom. 47 (2012) 1004–1014.
[38] B. Burla, M. Arita, M. Arita, A.K. Bendt, A. Cazenave-Gassiot, E.A. Dennis, K. Ekroos, X. Han, K. Ikeda, G. Liebisch, M.K. Lin, T.P. Loh, P.J. Meikle, M. Oresic, O. Quehenberger, A. Shevchenko, F. Torta, M.J.O. Wakelam, C.E. Wheelock, M.R. Wenk, MS-based lipidomics of human blood plasma: a community-initiated position paper to develop accepted guidelines, J. Lipid Res. 59 (2018) 2001–2017.
[39] N. El-Najjar, E. Orso, S. Wallner, G. Liebisch, G. Schmitz, Increased levels of sphingosylphosphorylcholine (SPC) in plasma of metabolic syndrome patients, PLoS One 10 (2015) e0140683.
[40] G. Tasseva, H.D. Bai, M. Davidescu, A. Haromy, E. Michelakis, J.E. Vance, Phosphatidylethanolamine deficiency in mammalian mitochondria impairs oxidative phosphorylation and alters mitochondrial morphology, J. Biol. Chem. 288 (2013) 4158–4173.
[41] K. Pfeiffer, V. Gohil, R.A. Stuart, C. Hunte, U. Brandt, M.L. Greenberg, H. Schagger, Cardiolipin stabilizes respiratory chain supercomplexes, J. Biol. Chem. 278 (2003) 52873–52880.

[42] A.K. Pollard, C.A. Ortori, R. Stoger, D.A. Barrett, L. Chakrabarti, Mouse mitochondrial lipid composition is defined by age in brain and muscle, Aging (Albany NY) 9 (2017) 986–998.
[43] S. Vankoningsloo, M. Piens, C. Lecocq, A. Gilson, A. De Pauw, P. Renard, C. Demazy, A. Houbion, M. Raes, T. Arnould, Mitochondrial dysfunction induces triglyceride accumulation in 3T3-L1 cells: role of fatty acid beta-oxidation and glucose, J. Lipid Res. 46 (2005) 1133–1149.
[44] P. Rockenfeller, M. Koska, F. Pietrocola, N. Minois, O. Knittelfelder, V. Sica, J. Franz, D. Carmona-Gutierrez, G. Kroemer, F. Madeo, Phosphatidylethanolamine positively regulates autophagy and longevity, Cell Death Differ. 22 (2015) 499–508.
[45] P.M. O'Connor, Renal oxygen delivery: matching delivery to metabolic demand, Clin. Exp. Pharmacol. Physiol. 33 (2006) 961–967.
[46] D.J. Pagliarini, S.E. Calvo, B. Chang, S.A. Sheth, S.B. Vafai, S.E. Ong, G.A. Walford, C. Sugiana, A. Boneh, W.K. Chen, D.E. Hill, M. Vidal, J.G. Evans, D.R. Thorburn, S.A. Carr, V.K. Mootha, A mitochondrial protein compendium elucidates complex i disease biology, Cell 134 (2008) 112–123.
[47] P. Bhargava, R.G. Schnellmann, Mitochondrial energetics in the kidney, Nat. Rev. Nephrol. 13 (2017) 629–646.
[48] M. Ren, C.K. Phoon, M. Schlame, Metabolism and function of mitochondrial cardiolipin, Prog. Lipid Res. 55 (2014) 1–16.
[49] G. Paradies, V. Paradies, V. De Benedictis, F.M. Ruggiero, G. Petrosillo, Functional role of cardiolipin in mitochondrial bioenergetics, Biochim. Biophys. Acta 1837 (2014) 408–417.
[50] Y. Shi, Emerging roles of cardiolipin remodeling in mitochondrial dysfunction associated with diabetes, obesity, and cardiovascular diseases, J. Biomed. Res. 24 (2010) 6–15.
[51] A. Broniec, R. Klosinski, A. Pawlak, M. Wrona-Krol, D. Thompson, T. Sarna, Interactions of plasmalogens and their diacyl analogs with singlet oxygen in selected model systems, Free Radic. Biol. Med. 50 (2011) 892–898.
[52] Z. Li, L.B. Agellon, T.M. Allen, M. Umeda, L. Jewell, A. Mason, D.E. Vance, The ratio of phosphatidylcholine to phosphatidylethanolamine influences membrane integrity and steatohepatitis, Cell Metab. 3 (2006) 321–331.
[53] A.B. Jordy, M.J. Kraakman, T. Gardner, E. Estevez, H.L. Kammoun, J.M. Weir, B. Kiens, P.J. Meikle, M.A. Febbraio, D.C. Henstridge, Analysis of the liver lipidome reveals insights into the protective effect of exercise on high-fat diet-induced hepatosteatosis in mice, Am. J. Physiol. Endocrinol. Metab 308 (2015) E778–E791.
[54] A.M. Lone, K. Tasken, Proinflammatory and immunoregulatory roles of eicosanoids in T cells, Front Immunol. 4 (2013) 130.
[55] J.M. van Dieren, Y. Simons-Oosterhuis, H.C. Raatgeep, D.J. Lindenbergh-Kortleve, M.E. Lambers, C.J. van der Woude, E.J. Kuipers, G.T. Snoek, R. Potman, H. Hammad, B.N. Lambrecht, J.N. Samsom, E.E. Nieuwenhuis, Anti-inflammatory actions of phosphatidylinositol, Eur. J. Immunol. 41 (2011) 1047–1057.
[56] L. Zhao, X. Zou, Z. Feng, C. Luo, J. Liu, H. Li, L. Chang, H. Wang, Y. Li, J. Long, F. Gao, J. Liu, Evidence for association of mitochondrial metabolism alteration with lipid accumulation in aging rats, Exp Gerontol. 56 (2014) 3–12.
[57] Z. Wang, Z. Ying, A. Bosy-Westphal, J. Zhang, B. Schautz, W. Later, S.B. Heymsfield, M.J. Muller, Specific metabolic rates of major organs and tissues across adulthood: evaluation by mechanistic model of resting energy expenditure, Am. J. Clin. Nutr. 92 (2010) 1369–1377.